Ultrasonics 96 (2019) 1–9

Contents lists available at ScienceDirect

Ultrasonics

journal homepage: www.elsevier.com/locate/ultras

Constitutive model of 6063 aluminum alloy under the ultrasonic vibration upsetting based on Johnson-Cook model

Zhendong Xie, Yanjin Guan*, Jun Lin, Jiqiang Zhai, Lihua Zhu

Key Laboratory for Liquid-Solid Structural Evolution and Processing of Materials (Ministry of Education), Shandong University, Jinan 250061, China

ARTICLE INFO

Keywords:
Ultrasonic vibration
Johnson-Cook model
Strain rate
Acoustic softening
Hardening

ABSTRACT

Establishing an accurate constitutive relation in ultrasonic vibration assisted metal forming, can provides a reliable theoretical basis for analyzing the mechanism of the ultrasonic vibration on materials. A constitutive model of 6063 aluminum alloy under the ultrasonic vibration upsetting at room temperature was constructed based on Johnson-Cook Model and experimental results. The influence of amplitude and frequency on the yield strength, hardening coefficient and exponent were analyzed quantitatively. Results showed that the yield strength was reduced due to the softening effect induced by the ultrasonic vibration. The maximum decreasing amount was 68.8% when imposing the maximum ultrasonic energy in this study. The hardening coefficient and exponent increased by 10.9% and 16.6% in maximum, respectively. However, the ultrasonic vibration has little impact on the strain rate hardening. The modified Johnson-Cook constitutive model under the ultrasonic vibration upsetting was established and was in good agreement with the experimental results.

1. Introduction

Considerable efforts are being devoted to the investigation of the ultrasonic vibration assisted metal plastic forming and its acting mechanism on materials in recent decades [1–3], and these developed forming processes, including ultrasonic drawing, ultrasonic extrusion and ultrasonic upsetting [4–6], has been widely used in practice.

Earlier studies [7–9] have shown that the influence of ultrasonic vibration on material properties mainly include two aspects: (1) the volume effect which can reduce the flow stress, and (2) the surface effect which affects the friction status between the die and the workpiece. Focusing on these two effects, many scholars have conducted various studies. However, the influence and acting mechanism of ultrasonic vibration on metals and theirs plastic behaviors are still unclear and the quantitative description model has not been established. Therefore, many efforts have been devoted to construct theoretical models that can quantitatively describe the effect of ultrasonic vibration on the plastic deformation behaviors of metals based on certain assumptions and simplification.

Atanasiu [10] systematically and quantitatively estimated the relation between the ultrasonic field and material properties, described the metal deformation behaviors in the process of ultrasonic assisted forming based on rigid-viscoplastic model and concluded that the yield strength of the material reduced exponentially with the increase of the ultrasonic intensity. Based on elastic-viscoplastic constitutive relation, He et al. [11] studied the variation of the uniaxial tensile stress and strain under the vibration condition. A one-dimensional mechanical model was established to describe the volume effect of low and medium frequency vibrations. They found that the vibrational tensile stress depends on the strain rate and strain history. According to the superposition principle and the strain variation assumption proposed by Kirchner, He et al. [12] also expressed a mathematical description of the volume effect, and they denoted that the physical nature of the volume effect was the decrease of the average stress. The influence of ultrasonic vibration on uniaxial tensile process depended on the frequency, amplitude and deformation velocity. Zheng et al. [13] studied the special behavior of metals under super-frequency vibration, and established the elastic constitutive equation of metals and emphasized that the effect of microstructures should be taken into account. According to the vibration assisted tensile experiments with applying low frequency vibration, Cai et al. [14] constructed a one-dimensional visco-elastoplastic model based on the Kirchner‘ assumption, and studied the mechanism of volume effect.

The above mentioned theoretical models only can reveal the influence of ultrasonic vibration on material behavior qualitatively and can’t describe the stress-strain relationship under the ultrasonic vibration condition quantificationally and accurately. Especially, the influence of the frequency and amplitude can’t be included into these theoretical

* Corresponding author.
E-mail address: guan_yanjin@sdu.edu.cn (Y. Guan).

https://doi.org/10.1016/j.ultras.2019.03.017
Received 19 June 2018; Received in revised form 28 November 2018; Accepted 20 March 2019
Available online 21 March 2019
0041-624X/

models. Thus, based on Arrhennius thermal activation model and dislocation evolution theory [15], Yao [16] proposed an acoustic softening model and an acoustic residual hardening model respectively. Upsetting tests assisted by high frequency vibration were conducted to construct the constitutive model of which the results showed a good agreement with the experimental results. Wang [17] divided the softening effect of ultrasonic vibration into two aspects: acoustic softening and stress superposition, and then calculated the proportion of the stress reduction induced by acoustic softening effect. Prabhakar et al. [18] also proposed a theoretical model based on the dislocation dynamics, which can express the effect of strain, strain rate and amplitude on the stress. However, there are too many parameters that are hard to obtain through the experiments in these models. Therefore, it is necessary to construct a relatively convenient and accurate theoretical model to reflect the stress-strain relationship of the material deformed under the ultrasonic vibration condition.

In general, an ideal model should be able to describe the materials' plastic behaviors, such as strain-rate dependence, temperature dependence, strain and strain-rate history dependence, work-hardening or strain-hardening behaviors. However, it is extremely difficult and even impossible to completely describe all these phenomena. Therefore, many scholars introduced necessary assumptions and tried to describe the deformation behavior in a wide range of strain rate and temperature as accurately as possible. At present, many phenomenological constitutive models are proposed which can well represent the materials' plastic deformation behaviors in a certain range, such as Johnson-Cook (JC) model [19], Zerilli-Armstrong model [20], Bodner-Partom model [21], and Khan-Huang model [22]. Especially, the JC constitutive model has been applied widely because of its simplicity and universality [23–25].

Therefore, in this paper, the conventional upsetting (C-upsetting) and ultrasonic vibration assisted upsetting (UV-upsetting) of 6063 Al alloy under different strain rates were conducted, and the parameters in the JC model were estimated based on the experimental results. The influence of the frequency and amplitude on material's parameters was analyzed. Consequently, the modified JC model which couples with the ultrasonic vibration parameters was established, which can reflect the influence of ultrasonic vibration on the stress-strain relation of 6063 Al alloy. This model provides a reliable theoretical basis for the analysis of the effect of ultrasonic vibration on the material deformation behaviors.

2. Original Johnson-Cook model

Johnson and Cook [19] proposed a constitutive model for metals subjected to large strains, high strain rates and high temperature in 1983. The JC constitutive model with simple form is purely empirical and has a clear physical explanation. On the other hand, the model includes less parameters which are easy to be obtained. In the JC model, the von Mises flow stress, σ is expressed as

$$\sigma = (C_1 + C_2\varepsilon^n)(1 + C_3 \ln \dot{\varepsilon}^*)(1 - T^{*m}) \tag{1}$$

where ε is the equivalent plastic strain, $\dot{\varepsilon}^*$ is the dimensionless strain rate and it is described as

$$\dot{\varepsilon}^* = \dot{\varepsilon}/\dot{\varepsilon}_r \tag{2}$$

where $\dot{\varepsilon}$ is the strain rate, $\dot{\varepsilon}_r$ is the reference strain rate under the quasi-static condition. The homologous temperature, T^* is written as:

$$T^* = (T - T_r)/(T_m - T_r) \tag{3}$$

where T is the deformation temperature, T_r is a reference temperature and T_m is the melting temperature of the material, all of which should be absolute temperature (K).

There are five material parameters in the JC model. C_1 is the yield stress at reference temperature and reference strain-rate, that is the stress resistance to micro plastic deformation. C_2 is the coefficient of strain-hardening, n is the strain-hardening exponent, indicating the strain hardening behavior of materials. C_3 is the coefficient of strain-rate hardening, reflecting the sensitivity of material to strain rate. m is the thermal softening exponent, meaning the softening effect of materials subjected to thermal loading. Because all of the experiments in our work were carried out at room temperature, $T = T_r$. Meanwhile, the factors of strain, strain-rate and temperature that in the JC model are independent of each other. Thus, the effect of the temperature can be ignored and then the JC model can be simplified as

$$\sigma = (C_1 + C_2\varepsilon^n)\left[1 + (C_3 \ln \frac{\dot{\varepsilon}}{\dot{\varepsilon}_r})\right] \tag{4}$$

In order to determine the parameters in (4), the upsetting tests under the reference strain-rate were performed firstly. When $\dot{\varepsilon} = \dot{\varepsilon}_r$, Eq. (4) can be simplified as

$$\sigma = (C_1 + C_2\varepsilon^n) \tag{5}$$

The value of C_1 is determined as the yield stress σ_s at the strain of 0.2% at the reference strain-rate. In this study, the reference strain rate $\dot{\varepsilon}_r$ is $3.33 \times 10^{-3}\,s^{-1}$.

By rearranging Eq. (5) and taking natural logarithm on both sides of Eq. (5), it could be transformed into the following form:

$$\ln(\sigma - \sigma_s) = n\ln\varepsilon + \ln C_2 \tag{6}$$

Then, using the true stress-strain data under reference strain-rate condition, the relationship between $\ln\varepsilon$ and $\ln((\sigma - \sigma_s))$ is determined. The values of n and C_2 can be obtained as the slope and intercept of the fitting line.

After that, several upsetting tests under a list of strain rates should be performed to obtain the unknown C_3.

It is found from Eq. (4) that the relationship between σ and $\ln(\dot{\varepsilon}/\dot{\varepsilon}_r)$ can be decided by flow stresses under different strain rates. The value of C_3 can be calculated from the slope $C_3 \cdot (C_1 + C_2\varepsilon^n)$ of the fitting line of σ-$\sigma_{0.2}$.

3. Ultrasonic vibration assisted upsetting

3.1. Establishment of ultrasonic vibration assisted upsetting system

The experimental system consists of a universal material testing machine (SANS CMT5205) and an ultrasonic vibration unit installed on the experimental machine by means of a frame, as shown in Fig. 1. The maximum load of the universal material testing machine is 200 kN, the crosshead speed is 0.001–250 mm/min. In the present work, the ultrasonic vibration unit includes ultrasonic generator, transducer, amplitude transformer and tool head. The transducer converts the high frequency electric oscillation generated by the ultrasonic power into the mechanical vibration. However, the amplitude of the output mechanical vibration is very small, so it needs to be amplified by using the amplitude transformer. Finally, the ultrasonic vibration acts on the upsetting specimens through the tool head.

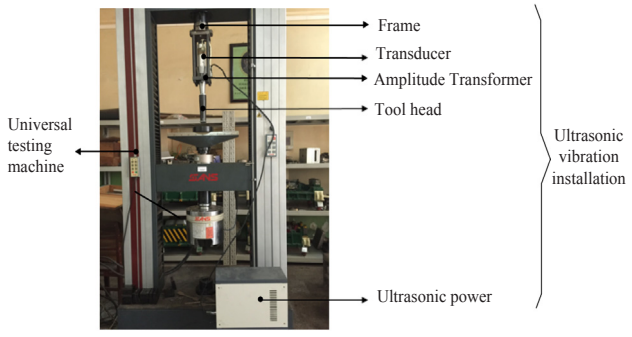

Fig. 1. Ultrasonic assisted upsetting test system.

Table 1
Chemical composition of 6063 aluminum alloy (wt%).

Element	Si	Fe	Cu	Mn	Mg	Zn	Ti	Cr	Other	Al
Content	0.32	0.35	0.1	0.1	0.6	0.1	0.1	0.1	0.05	Balance

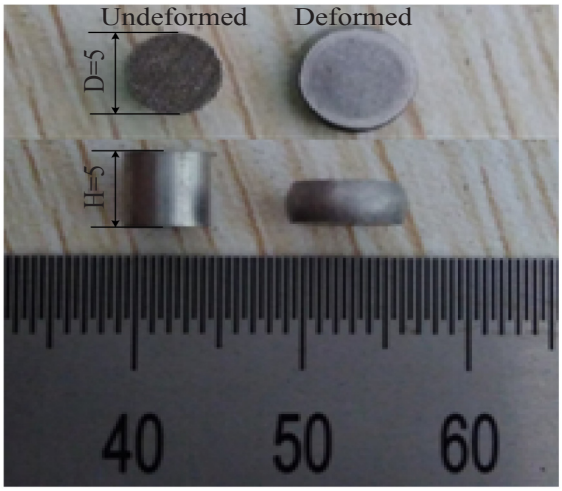

Fig. 2. Upsetting specimen.

3.2. Compression specimens and treatment

Table 1 gives the chemical composition of the 6063 aluminum alloy used in the tests. The specimen dimension is Φ5 mm × 5 mm, as shown in Fig. 2.

In order to eliminate the residual stress caused by machining operations and ensure the consistency of the microstructures and performances of specimens, a recrystallization annealing process was conducted for the 6063 aluminum alloy specimens. The specimens were heated to 500 °C at the heating rate of 5 °C/min and then cooled down to the room temperature in a furnace after 4 h heat preservation. The specimens were buried in the alumina powder to prevent from oxidization during the annealing process.

3.3. Upsetting test schemes

Upsetting tests were conducted on as annealed 6063 aluminum alloy bars under different strain rates and vibration conditions to calculate the parameters in the JC model. The upsetting reduction is 50%. The strain rates are set as $3.33 \times 10^{-3}\,s^{-1}$, $1.0 \times 10^{-2}\,s^{-1}$, $0.1\,s^{-1}$ and $0.8\,s^{-1}$, respectively. As shown in Table 2, ultrasonic vibration with different frequencies and amplitudes were applied in the upsetting process. When the load reached to 1 kN until the reduction in height was 2.5 mm. Each experiment was repeated three times in order to guarantee the reliability of the experimental results.

4. Constitutive modeling

4.1. Influence of the strain rate and ultrasonic vibration on the deformation behavior

The C-upsetting and UV-upsetting were performed according to the test schemes. Fig. 3 shows the stress-strain curves under various strain rates and ultrasonic vibration conditions. Aluminum alloy 6063 is a rate sensitive material [26]. There is not enough time for grain rotation, grain boundary sliding and the dislocation movement with the increase of the strain rate. Thus, the plastic deformation can't be conducted sufficiently, and that induce the increase of the true stress [27]. Obviously, the true stress increased with the increases of the strain rate whether the ultrasonic vibration was imposed in upsetting process or not.

Table 2
The ultrasonic parameter.

Frequency/kHz	15					20		28			
Amplitude/μm	3.34	3.96	4.48	4.96	5.39	4.6	6	3	3.6	4.32	4.81

The flow stress reduced immediately at the moment of applying the ultrasonic vibration, and the decreasing range of the stress is related to the vibration amplitude and frequency [9,28]. Furthermore, the surface effect induced by the ultrasonic vibration effectively improves the lubrication condition between the specimen and the die and then the friction decreases [29,30], which is helpful to material's flow and contributes to the stress reduction. Table 3 lists the yield strengths under different vibration frequencies and amplitudes when $\Delta\sigma_{0.5}$ is $3.33 \times 10^{-3}\,s^{-1}$. Obviously, the deformation behavior of the materials changes significantly after applying the ultrasonic vibration, which indicates besides the strain rate the deformation behavior of the materials is closely related to the ultrasonic vibration.

Generally, the upsetting process can be divided into elastic deformation stage, yielding stage and plastic deformation stage. The forming process is using plastic deformation of the metal and the ultrasonic vibration bring more obvious influences on the stress-strain relationship of plastic deformation. So, the stress-strain relationship in plastic deformation stage was analyzed to study the effect of ultrasonic vibration on the material properties during plastic deformation.

The stress when the strains are 0.2 and 0.5, $\sigma_{0.2}$ and $\sigma_{0.5}$ are extracted from the stress-strain curves under different strain rates, respectively. The stress differences $\Delta\sigma_{0.2}$ and $\Delta\sigma_{0.5}$ between the flow stresses under a specified strain rate and ones under the reference strain rate $\Delta\sigma_{0.5} = 3.33 \times 10^{-3}\,s^{-1}$ are calculated and demonstrated in Fig. 4 as an example when the strain rate is $0.1\,s^{-1}$ under different ultrasonic vibration conditions. Table 4 displays the values of $\Delta\sigma_{0.2}$, $\Delta\sigma_{0.5}$ and $\Delta\sigma = \Delta\sigma_{0.5} - \Delta\sigma_{0.2}$ under different strain rates.

From the Table 4, it can be found that $\Delta\sigma_{0.5} > \Delta\sigma_{0.2}$ for all strain rates, and $\Delta\sigma$ increases with the increases of strain rate. When the strain rate is constant, $\Delta\sigma$ under the effect of ultrasonic vibration is larger than that of without ultrasonic vibration, as shown in Fig. 5. In plastic deformation stage, the hardening of material is getting more obvious after applying the ultrasonic vibration, and the hardening is related with the input ultrasonic energy in unit time.

An average stress gradient in plastic deformation stage of which under different strain rate is defined for quantitatively analyzing the hardening effect of ultrasonic vibration, it is expressed as

$$K_{av} = \frac{\sigma_{0.5} - \sigma_{0.2}}{\Delta\varepsilon} \tag{7}$$

where, $\Delta\varepsilon = 0.5 - 0.2 = 0.3$.

Fig. 6 shows the variations of average stress gradient with the amplitudes when the frequencies are 15 kHz and 28 kHz, respectively. Clearly, the average stress gradient increases with the increasing amplitude and became larger with the increase of the frequency when the amplitude keeps invariable. To some extent, the average stress gradient represents the hardening degree. Thus, the larger the amplitude or frequency is, the more obvious hardening effect can be found.

4.2. Solution of conventional JC model

In order to establish the constitutive model under the ultrasonic vibration condition, it is needed to calculate the parameters in JC model based on the stress strain curves that obtained from conventional and ultrasonic vibration assisted upsetting.

In the present study, $C_1 = 69$ MPa is the yield strength when the compressive strain rate is $3.33 \times 10^{-3}\,s^{-1}$, as shown in Table 3.

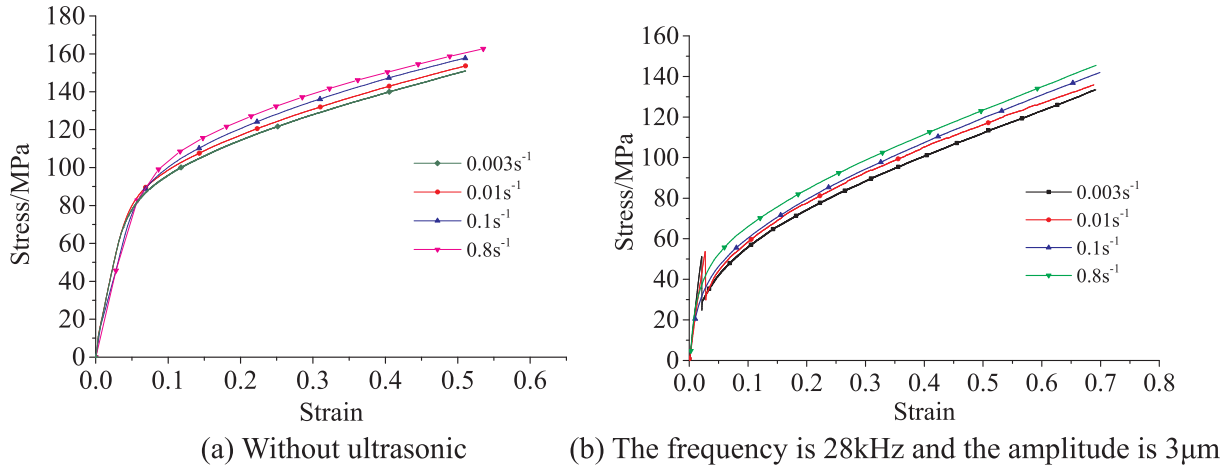

Fig. 3. The stress-strain curves under different strain rates.

Table 3
The yield strengths under different ultrasonic vibration conditions.

Frequency/kHz	-	15					20		28			
Amplitude/μm	-	3.34	3.96	4.48	4.96	5.39	4.6	6	3	3.6	4.32	4.81
Yield strength/MPa	69	45.5	44.2	42.3	40.8	39.4	35.2	27.7	30.1	27.1	23.7	21.5

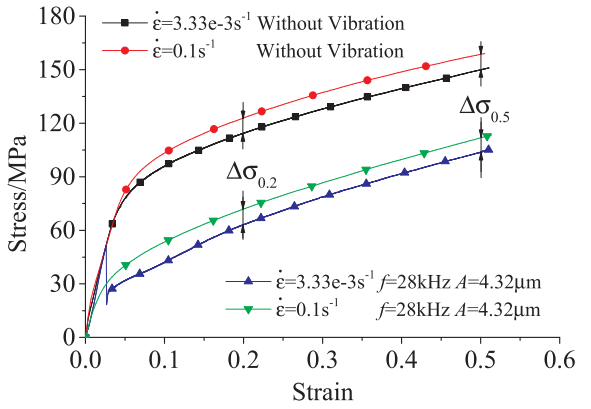

Fig. 4. Demonstration of $\Delta\sigma_{0.2}$ and $\Delta\sigma_{0.5}$ when the strain rate is 0.1 s^{-1}.

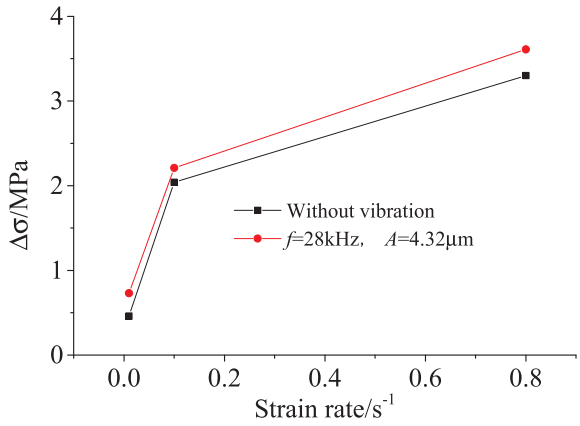

Fig. 5. The variation of $\Delta\sigma$ with different strain rate.

Table 4
The values of $\Delta\sigma_{0.2}$ and $\Delta\sigma_{0.5}$ under different strain rates.

Vibration condition	Without vibration			f = 28 kHz, A = 4.32 μm		
Strain rate/s^{-1}	0.01	0.1	0.8	0.01	0.1	0.8
$\Delta\sigma_{0.2}$/MPa	2.27	6.2	10.3	1.09	3.56	5.92
$\Delta\sigma_{0.5}$/MPa	2.73	8.24	13.6	1.82	5.77	9.53
$\Delta\sigma$/MPa	0.46	2.04	3.3	0.73	2.21	3.61

Substituting 69 MPa into Eq. (6), the curve of $\ln(\sigma - 69)$ - $\ln\varepsilon$ can be obtained shown in Fig. 7. And the curves in plastic deformation stage are linearly fitted to calculate the C_2 and n.

In order to obtain strain rate sensitivity coefficient C_3, nine groups of stress values, of which corresponding strains are 0.1, 0.15, 0.2, 0.25, 0.3, 0.35, 0.4, 0.45 and 0.5 respectively, were adopted under different strain rates. Linear fitting results between σ and $\ln(\dot{\varepsilon}/\dot{\varepsilon}_r)$ can be gotten based on experimental data, as shown in Fig. 8. Then, the values of C_3 under different strains can be obtained by calculating the slopes of the $\sigma - \ln(\dot{\varepsilon}/\dot{\varepsilon}_r)$ lines. Consequently, the average value is taken as the final C_3, as shown in Table 5.

The values of C_1, C_2, C_3 and n under different ultrasonic vibration were calculated according to the solution process that described above,

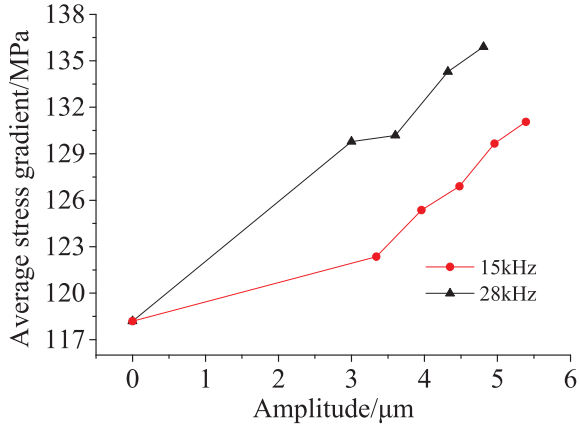

Fig. 6. Variations of average stress gradient with the amplitudes.

as shown in Table 6. The correlation coefficients between C_1, C_2, C_3, n and amplitude are −0.997, 0.993, 0.081, 0.983, respectively when the frequency is 15 kHz and are −0.991, 0.994, 0.106, 0.992 when the

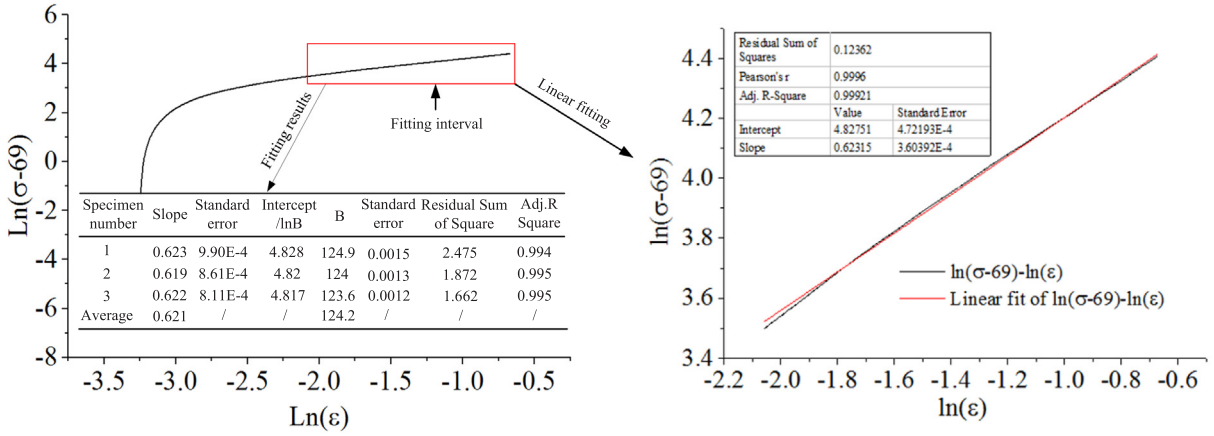

Fig. 7. Fitting interval and fitting results of conventional upsetting results.

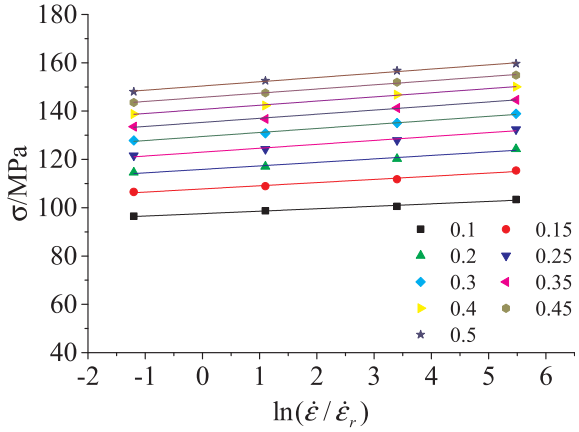

Fig. 8. Linear fitting of $\sigma - \ln(\dot{\varepsilon}/\dot{\varepsilon}_r)$ without ultrasonic vibration.

Table 5
Results of linear fitting of $\sigma - \ln(\dot{\varepsilon}/\dot{\varepsilon}_r)$ without ultrasonic vibration.

Strain	Slope	Standard Error	Intercept	Standard Error	Adj. R Square	Residual Sum of Square	C_3
0.1	1.012	0.07987	97.556	0.266	0.982	0.319	0.0143
0.15	1.314	0.10862	107.785	0.361	0.98	0.589	0.0162
0.2	1.442	0.13665	115.882	0.454	0.974	0.933	0.0165
0.25	1.616	0.15492	123.019	0.515	0.973	1.198	0.017
0.3	1.672	0.10017	129.485	0.333	0.989	0.501	0.0169
0.35	1.695	0.07912	135.392	0.263	0.994	0.313	0.0164
0.4	1.72	0.05509	140.730	0.183	0.997	0.152	0.016
0.45	1.721	0.06931	145.723	0.231	0.995	0.24	0.0155
0.5	1.75	0.09234	150.418	0.307	0.992	0.426	0.0157
Average							0.0161

Table 6.1
Material constants without ultrasonic vibration.

Without ultrasonic	C_1/MPa	C_2/MPa	n	C_3
—	69	124.2	0.621	0.0161

frequency is 28 kHz.

The JC model of 6063 aluminum alloy materials during the upsetting without ultrasonic vibration is expressed as

$$\sigma = (69 + 124.2\varepsilon^{0.621})\left(1 + 0.0161 \ln \frac{\dot{\varepsilon}}{\dot{\varepsilon}_r}\right) \quad (8)$$

Table 6.2
Material constants when the frequency is 15 kHz.

Amplitude/μm	C_1/MPa	C_2/MPa	n	C_3
3.34	45.5	127.8	0.631	0.0162
3.96	44.2	129.5	0.636	0.016
4.48	42.3	130.3	0.643	0.0158
4.96	40.8	131.8	0.651	0.0165
5.39	39.4	133	0.656	0.0163

Table 6.3
Material constants when the frequency is 20 kHz.

Amplitude/μm	C_1/MPa	C_2/MPa	n	C_3
4.6	35.2	131.7	0.668	0.016
6	27.7	136.8	0.708	0.0163

Table 6.4
Material constants when the frequency is 28 kHz.

Amplitude/μm	C_1/MPa	C_2/MPa	n	C_3
3	30.1	132.9	0.681	0.016
3.6	27.1	134.4	0.697	0.0165
4.32	23.7	136.8	0.711	0.0164
4.81	21.5	137.7	0.724	0.0159

4.3. The modified JC model for ultrasonic vibration assisted upsetting

The modified JC model of 6063 aluminium alloy UV-upsetting was constructed based on the experimental values of C_1, C_2, C_3 and n, under different frequencies and amplitudes.

Firstly, under a certain frequency, the influence of the amplitude on material parameters was studied. Since the ultrasonic vibration equipment with frequency 20 kHz only provides two kinds of amplitudes, 4.6 μm and 6 μm, and there are fewer parameters, it is unable to do regularity analysis. Thus, the influence of amplitude on material parameters in the JC model was studied when the frequency are 15 kHz and 28 kHz, respectively.

For convenience, C_{10}, C_{20}, C_{30} and n_0 represent the JC model parameters of C-upsetting, and C_{1v}, C_{2v}, C_{3v} and n_v respectively represent those of UV-upsetting. In order to study the influence of amplitude on material parameters in the JC model, variations of C_{10}/C_{1v}, C_{2v}/C_{20}, n_v/n_0 and C_{3v}/C_{30} with different vibration parameters were obtained respectively, as shown in Fig. 9.

It can be seen from the Fig. 9, when the frequency keeps invariable, the C_{10}/C_{1v} increases with the increase of the amplitude, and the relationship between them is not simply linear but approximately

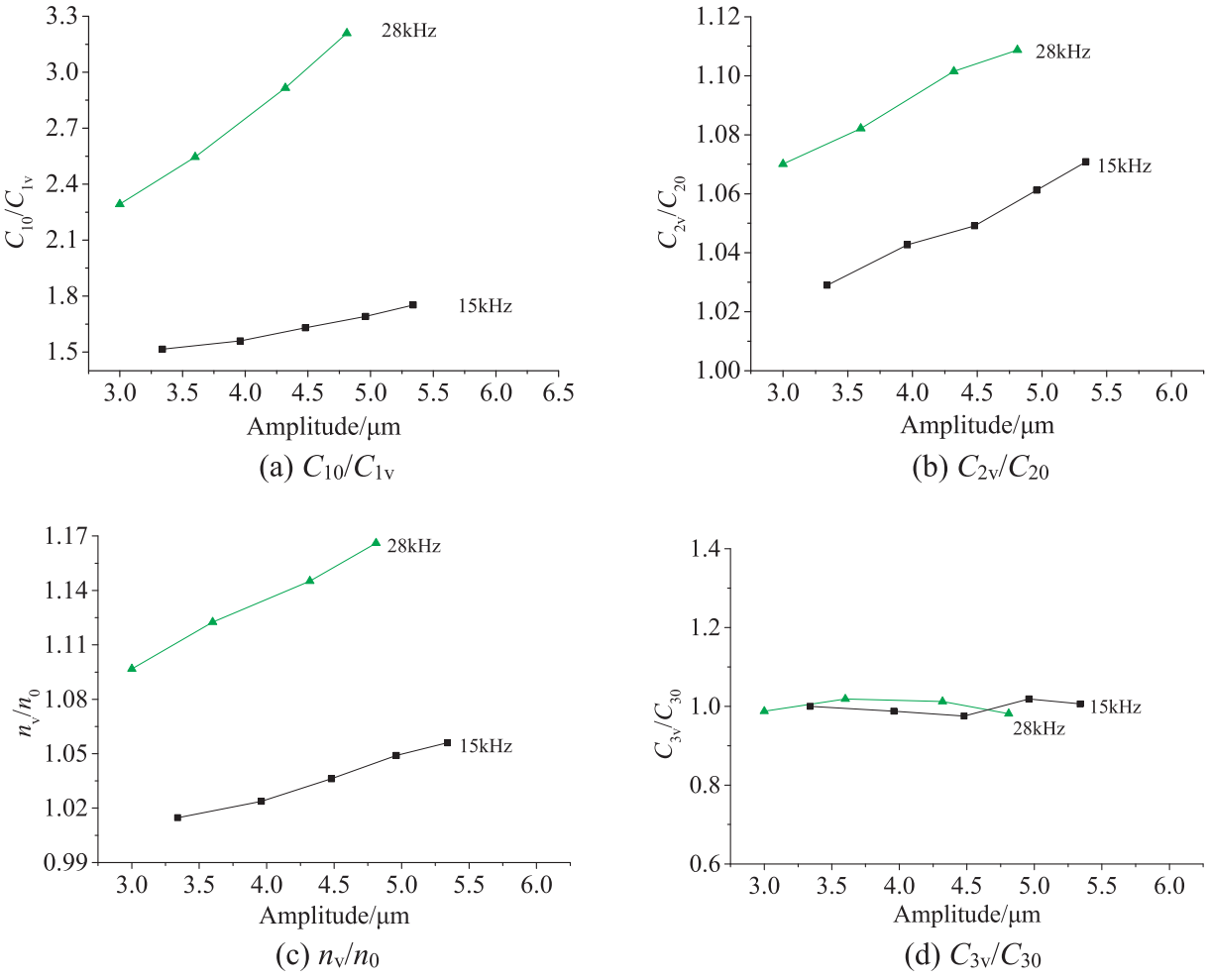

Fig. 9. Variations of C_{10}/C_{1v}, C_{2v}/C_{20}, n_v/n_0 and C_{3v}/C_{30} with different vibration.

exponential [10]. C_{2v}/C_{20} and n_v/n_0 increase linearly with the increase of amplitude. Clearly, all of n_i/n_0 and C_{2v}/C_{20} are larger than 1.0 after applying the ultrasonic vibration, which reveals the application of the ultrasonic vibration intensifies the material hardening and both the hardening coefficient and the hardening exponent increase with the increase of the amplitude. C_{3v}/C_{30} is basically around 1.0 under different amplitudes, which means that the ultrasonic vibration has little effects on C_3. Therefore, C_3 is considered as a constant of 0.0162 according to the average result of all upsetting tests.

Based on the varying trends of C_{10}/C_{1v}, C_{2v}/C_{20} and n_v/n_0 with the amplitudes, the following relationships can be proposed:

$$C_{10}/C_{1v} = e^{aA} + b \tag{9-1}$$

$$C_{2v}/C_{20} = k_1 A + l_1 \tag{9-2}$$

$$n_v/n_0 = k_2 A + l_2 \tag{9-3}$$

where A is the amplitude, a, b, k_1, k_2, l_1 and l_2 are contants which can be determined according to the experimental data. They can be obtained by fitting curves in Fig. 9, as listed in Table 7.

Then, the modified JC models that coupled with the amplitude under frequencies of 15 kHz and 28 kHz can be expressed as Eqs. (10-1) and (10-2), respectively.

$$\sigma = \left[\frac{69}{\exp(0.112A) - 0.0259} + (2.52A + 119.4)\right.$$
$$\left.\varepsilon^{(0.0081A+0.605)}\right]\left[1 + 0.0162\ln\frac{\dot{\varepsilon}}{\dot{\varepsilon}_r}\right] \tag{10-1}$$

$$\sigma = \left[\frac{69}{\exp(0.21A) + 0.479} + (2.75A + 124.6)\right.$$
$$\left.\varepsilon^{(0.0232A+0.612)}\right]\left[1 + (0.0162\ln\frac{\dot{\varepsilon}}{\dot{\varepsilon}_r})\right] \tag{10-2}$$

Based on Eq. (10), stress-strain relations under different amplitudes and strain rates are calculated and compared with the corresponding experimental results in Fig. 10. Obviously, The predicted results using the proposed JC model show good agreement with the experimental results, and the maximum error is only 5.71%. The values of a, k_1 and k_2 in the Eq. (9) under 28 kHz are greater than those under 15 kHz which reveals that the ultrasonic vibration with a higher frequency has a more significant impact on the parameters in the modified JC model.

Besides amplitude, the frequency of ultrasonic vibration also has an impact on the material parameters of the JC model. The constitutive model under the ultrasonic vibration condition should consider the parameters of frequency and amplitude synthetically. Thus, based on the data listed in Table 6, the constitutive model of coupling with the frequency and amplitude can be established.

Based on the Eq. (10), the decrease of yield strength is exponentially related to the ultrasonic energy, and the ultrasonic energy $I \propto A^2 f^2$. Moreover, the hardening coefficient and the hardening exponent were assumed increasing linearly with the increase of the amplitude. In the

Table 7
The constants of which the frequency are 15 kHz and 28 kHz.

Frequency/kHz	a	b	k_1	l_1	k_2	l_2
15	0.112	−0.0259	2.52	119.4	0.0081	0.605
28	0.21	0.479	2.75	124.6	0.0232	0.612

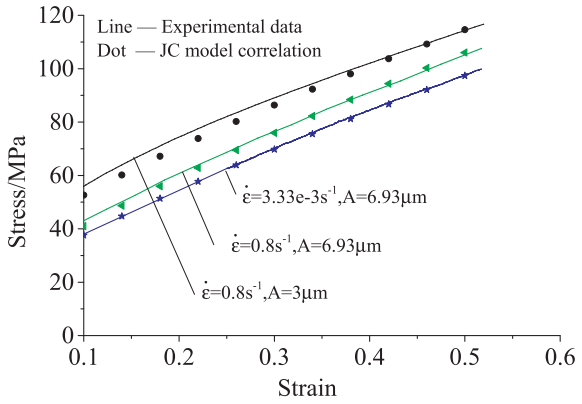

Fig. 10. Comparison between the flow stresses calculated from the JC model and the flow stresses measured from experimental data when the frequency is 28 kHz.

meanwhile, the ratio of the yield strengths before and after applying the ultrasonic vibration is in linear relationship with the ultrasonic energy, amplitude and frequency.

$$C_{10}/C_{1v} = \alpha_1 A^2 f^2 + \alpha_2 A + \alpha_3 f + \alpha_4 \tag{11-1}$$

$$C_{2v}/C_{20} = \beta_1 A + \beta_2 f + \beta_3 \tag{11-2}$$

$$n_v/n_0 = \eta_1 A + \eta_2 f + \eta_3 \tag{11-3}$$

Fig. 11 shows the fitting surfaces of C_{10}/C_{1v}, C_{2v}/C_{20} and n_v/n_0, and the points represent the experimental data under different frequencies and amplitudes. The calculated results show good agreement with the upsetting experimental data. Table 8 gives the fitting results of the parameters defined in the Eq. (11). The value of C_3 still remains invariable under different frequencies, so that $C_3 = 0.0162$. Finally, the modified JC constitutive model of ultrasonic vibration assisted 6063 aluminum alloy upsetting can be expressed as Eq. (12).

$$\sigma = [\frac{69}{7.13\times10^{-5}A^2f^2 + 0.0145A + 0.0423f + 0.601} + (2.571A + 0.478f + 111.9)\varepsilon^{0.0182A+0.00536f+0.482}](1 + 0.0162ln\frac{\dot{\varepsilon}}{\dot{\varepsilon}_r}) \tag{12}$$

According to the Eq. (12), the stress-strain relations at different frequencies and amplitudes were calculated and compared with experimental results, as shown in Fig. 12. Clearly, both of them are in good agreement, the maximum error is only 5.71%, which shows a high accuracy of the modified JC model and can accurately describe the stress-strain relationship under the ultrasonic vibration condition. Meanwhile, from the Eq. (12), it can be found that when the amplitude keeps invariable, the stress decreasing range increases with the increase of the frequency, and the hardening coefficient and hardening effect exponent also increase linearly with the increasing frequency, which indicates material's softening and hardening are intensified with the increase of the frequency.

From Fig. 10 and Fig. 12, both the frequency and amplitude have a certain impact on stress-strain curve that is sensitive to the change of the frequency and amplitude. Therefore, in order to study the influence of the frequency or amplitude on the material's deformation behavior, partial derivatives of Eq. (11) with respect to frequency and amplitude

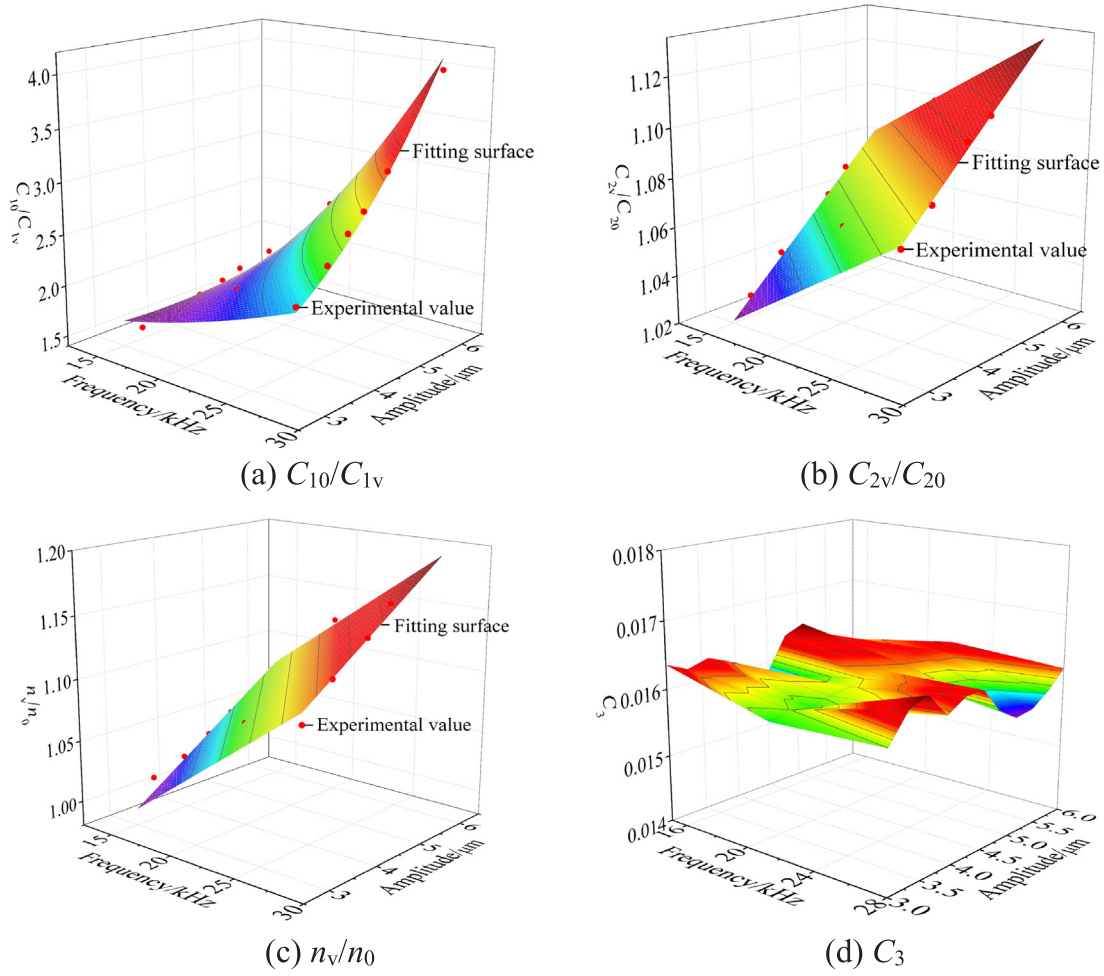

Fig. 11. Variations of C_{10}/C_{1v}, C_{2v}/C_{20} and n_v/n_0 with the frequency and amplitude.

Table 8
Constants in Eq. (11).

Constants	α_1	α_2	α_3	α_4	β_1	β_2	β_3	η_1	η_2	η_3
value	7.13×10^{-5}	0.0145	0.0423	0.601	0.0207	0.00385	0.901	0.0293	0.00863	0.776

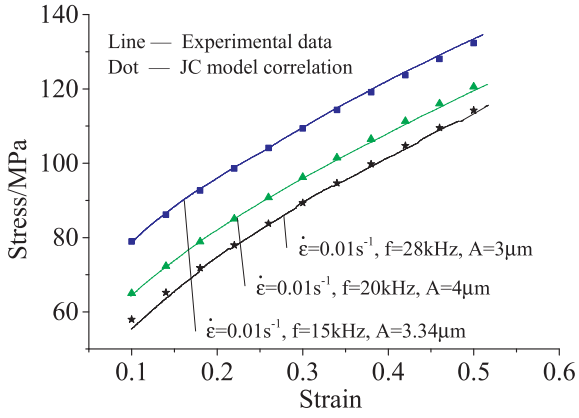

Fig. 12. Comparison between the flow stresses calculated from the JC model and the flow stresses measured from experimental data at different ultrasonic vibration conditions.

are obtained respectively.

$$\partial(C_{10}/C_{1v})/\partial f = 2\alpha_1 A^2 f + \alpha_3,\ \partial(C_{10}/C_{1v})/\partial A = 2\alpha_1 A f^2 + \alpha_2 \quad (13\text{-}1)$$

$$\partial(C_{2v}/C_{20})/\partial f = \beta_2,\ \partial(C_{2v}/C_{20})/\partial A = \beta_1 \quad (13\text{-}2)$$

$$\partial(n_v/n_0)/\partial f = \eta_2,\ \partial(n_v/n_0)/\partial A = \eta_1 \quad (13\text{-}3)$$

Eq. (13-1) reflects the sensitivity of the yield strength to the frequency and amplitude. Table 9 shows the values of $\partial(C_{10}/C_{1v})/\partial f$ and $\partial(C_{10}/C_{1v})/\partial A$ under different frequencies and amplitudes. For the same frequency and amplitude, $\partial(C_{10}/C_{1v})/\partial A > \partial(C_{10}/C_{1v})/\partial f$, which indicates that the influence of amplitude on the yield strength is greater than that of frequency. Eqs. (13-2) and (13-3) reflect the sensitivity of the hardening coefficient and hardening exponent to the frequency and amplitude, respectively. Table 8 shows $\beta_1 > \beta_2$ and $\eta_1 > \eta_2$, which reveals the hardening coefficient and hardening exponent are more sensitive to the variation of amplitude than that of frequency. The influence of amplitude on the hardening effect is more significant.

Due to the volume and surface effects induced by the ultrasonic vibration, the material's stress-strain relationship changes significantly, the yield strength of the material reduces. It can be seen from the Eq. (12) that C_1 related with the yield strength decreases with the increase of frequency and amplitude, i.e., material's yield strength reduces with the increase of the ultrasonic intensity. This is because there are a large number of defects in the material crystals, including voids, dislocations and grain boundaries, a part of ultrasonic vibration energy can be absorbed by these defects when the ultrasonic travelling through the material. The material can absorb more ultrasonic vibration energy under the effect of high-density ultrasonic energy and the dislocations are easy to be excitated, motion and propagation of dislocations occur even if the stress is small. And then it shows the forming load decreases on macro level [31–33]. Meanwhile, the application of the ultrasonic vibration can also produce the effect of stress superposition, which makes the flow stress reduced to some extent. On the other hand, the friction condition on the specimen/tool interface was improved due to the surface effect induced by the ultrasonic vibration [34,35], which also contributes to the decrease of the forming load.

The hardening coefficient C_2 and the hardening exponent n increase linearly with the increase of amplitude and frequency. It shows that the application of the ultrasonic vibration has not only softening effect but also hardening effect on the material. The hardening mechanism of the ultrasonic vibration on the material includes three aspects: (1) The deformation of the crystal is no longer the slip between the slip planes and a certain distortion occurs between the crystal planes when the ultrasonic vibration energy is high enough, which causes the material's hardening [7]. (2) While promoting dislocation motion and propagation, the absorbed ultrasonic vibration energy makes the material produce dislocation tangle and result in a certain hardening of the material. The greater the inputting ultrasonic energy per unit time is, the more obvious the hardening of the materail is. (3) The material is subjected to the ultrasonic vibration with high frequency and produces asymmetrical cyclic deformation, which leads to the cyclic hardening of material [36,37].

The 6063 aluminium alloy is a strain rate sensitive material. The instantaneous strain rate of the material changes periodically under the ultrasonic vibration condition, its direction was by turns in the same and the opposite as the compressed direction [38]. The instantaneous strain rate increases with the increase of the frequency and amplitude. Thanks to the flow direction of material is periodic, the average strain rate of the material does not change in the whole deformation process. Thus, the ultrasonic vibration has little effect on the strain rate constant C_3.

5. Conclusions

The constitutive equation of 6063 aluminum alloy under the ultrasonic vibration was constructed based on the Johnson-Cook Model. The influence of amplitude and frequency on yield strength, strain hardening coefficient and strain hardening exponent of the alloy was quantitatively analyzed. The main conclusions are as follows:

Ultrasonic vibration has softening effect on materials, which shows the decrease of the yield stress C_1. The decreasing range increases with the increase of the inputting ultrasonic energy in unit time. The influence of amplitude on the softening effect is greater than that of frequency.

Besides the softening effect, the ultrasonic vibration has hardening effect on materials, which shows the curve slope of the plastic deformation stage increases. The hardening coefficient C_2 and the hardening exponent n increase linearly with the increase of

Table 9
The values of $\partial(C_{10}/C_{1v})/\partial f$ and $\partial(C_{10}/C_{1v})/\partial A$ under different frequencies and amplitudes.

Frequency/kHz	15					20		28			
Amplitude/μm	3.34	3.96	4.48	4.96	5.39	4.6	6	3	3.6	4.32	4.81
$\frac{\partial(C_{10}/C_{1v})}{\partial f}$	0.0666	0.0758	0.0852	0.0949	0.104	0.0879	0.145	0.0782	0.094	0.117	0.135
$\frac{\partial(C_{10}/C_{1v})}{\partial A}$	0.122	0.142	0.158	0.174	0.187	0.243	0.357	0.35	0.417	0.497	0.552

amplitude or frequency. The influence of amplitude on the hardening effect is greater than that of frequency.

Under different ultrasonic vibration, the coefficient of strain-rate hardening basically remains invariable, which shows the ultrasonic vibration has little effect on the C_3.

Based on the experimental and calculating results, the new constitutive model shows a good agreement with the upsetting experiment results, the maximum error of the new constitutive model is just 5.71%.

Acknowledgments

The research work was supported by the National Natural Science Foundation of China (Approval No: 51675307, 51375269, 51705291).

References

[1] A.E. Eaves, A.W. Smith, W.J. Waterhouse, D.H. Sansome, Review of the application of ultrasonic vibrations to deforming metals, Ultrasonics 13 (1975) 162–170.
[2] C. Zha, W. Chen, Q. Xu, Ultrasonic vibration assisted micro-froming process and its current situation analysis, Hot Work. Tech. 46 (9) (2017) 18–22.
[3] S. Kumar, C.S. Wu, G.K. Padhy, W. Ding, Application of ultrasonic vibrations in welding and metal processing: A status review, J. Manuf. Processes 26 (2017) 295–322.
[4] K. Siegert, A. Möck, Wire drawing with ultrasonically oscillating dies, J. Mater. Proc. Tech. 60 (1996) 657–660.
[5] S.A.A.A. Mousavi, H. Feizi, R. Madoliat, Investigations on the effects of ultrasonic vibrations in the extrusion process, J. Mater. Proc. Tech. 187–188 (2007) 657–661.
[6] T. Jimma, Y. Kasuga, N. Iwaki, O. Miyazawa, E. Mori, K. Ito, H. Hatano, An application of ultrasonic vibration to the deep drawing process, J. Mater. Proc. Tech. 80–81 (1998) 406–412.
[7] B. Langenecker, Effects of ultrasound on deformation characteristics of metals, IEEE T. Sonics and Ultrasonics 13 (1966) 1–8.
[8] S. Abdul Aziz, M. Lucas, The effect of ultrasonic excitation in metal forming tests, Appl. Mech. Mater., Trans. Tech. Publ. (2010) 311–316.
[9] Y. Daud, M. Lucas, Z. Huang, Modelling the effects of superimposed ultrasonic vibrations on tension and compression tests of aluminium, J. Mater. Proc. Tech. 186 (2007) 179–190.
[10] N. Atanasiu, Metal forming in the ultrasonic field, Advanced Technology of Plasticity, Proceedings of ICTP-2, ICTP, Tokyo, 1984, pp. 799–804.
[11] Q. He, B. Wen, Mechanism on volume effect in metals plastic processes with vibration, Metal .Form. Tech. 16 (6) (1998) 35–36.
[12] Q. He, B. Wen, An elastic-viscoplastic model for the tension under oscillatory loading, Mech. Sci. Tech. 19 (3) (2000) 345–346 352.
[13] J. Zheng, H. Hu, J. Cheng, Analysis of constitutive relation of materials under UHF vibration, J. Harbin Inst. Tech. 29 (1) (1997) 6–9.
[14] G. Cai, Z. Jiang, H. Weng, Volume effect analysis of visco-elasticity models for plastic deformation with low-frequency vibration, J. Mech. Strength 29 (2) (2007) 346–350.
[15] U.F. Kocks, Constitutive behavior based on crystal plasticity, in: A.K. Miller (Ed.), Unified Constitutive Equations for Creep and Plasticity, Elsevier Applied Science, London; New York, 1987, pp. 1–88.
[16] Z. Yao, G. Kim, Z. Wang, L. Faidley, Q. Zou, D. Mei, Z. Chen, Acoustic softening and residual hardening in aluminum: Modeling and experiments, Int. J. Plasticity 39 (2012) 75–87.
[17] C.J. Wang, Y. Liu, B. Guo, D.B. Shan, B. Zhang, Acoustic softening and stress superposition in ultrasonic vibration assisted uniaxial tension of copper foil: Experiments and modeling, Mater. Design 112 (2012) 246–253.
[18] A. Prabhakar, G.C. Verma, H. Krishnasamy, P.M. Pandey, M.G. Lee, S. Suwas, Dislocation density based constitutive model for ultrasonic assisted deformation, Mech. Res. Commun. 85 (2017) 76–80.
[19] G.R. Johnson, W.H. Cook, A constitutive model and data for metals subjected to large strains, high strain rates and high temperatures, Proceedings of the 7th International Symposium on Ballistics, 1983, pp. 541–547.
[20] F.J. Zerilli, R.W. Armstrong, Dislocation-mechanics-based constitutive relations for material dynamics calculations, J. Appl. Phys. 61 (1987) 1816–1825.
[21] S.R. Bodner, Y. Partom, Constitutive equation for elastoviscoplastic strain hardening material, ASME J. Appl. Mech. 385–389 (1975).
[22] A.S. Khan, S. Huang, Experimental and theoretical study of mechanical behavior of 1100 aluminum in the strain rate range 10^{-5}-10^{4} s^{-1}, Int. J. Plasticity 8 (1992) 397–424.
[23] Z. Li, M. Zhan, X. Fan, J. Tan, A modified Johnson-Cook model of as-quenched AA2219 considering negative to positive strain rate sensitivities over a wide temperature range, Proc. Eng. 207 (2017) 155–160.
[24] V. Sampsa, N. Esko, Modified Johnson-Cook flow stress model with thermal softening damping for finite element modeling of cutting, P. I. Mech. Eng. B-J Eng. 230 (2016) 241–253.
[25] Y. Zhang, S. Yao, X. Hong, Z. Wang, A modified Johnson-Cook model for 7N01 aluminum alloy under dynamic condition, J. Cent. South Univ. 24 (2017) 2550–2555.
[26] Q. Wei, S. Cheng, K.T. Ramesh, E. Ma, Effect of nanocrystalline and ultrafine grain sizes on the strain rate sensitivity and activation volume: fcc versus bcc metals, Mat. Sci. Eng. A 381 (2004) 71–79.
[27] J.R. Klepaczko, C.Y. Chiem, On rate sensitivity of f.c.c. metals, instantaneous rate sensitivity and rate sensitivity of strain hardening, J. Mech. Phys. Solids 34 (1986) 29–54.
[28] R. Pohlman, E. Lehfeldt, Influence of ultrasonic vibration on metallic friction, Ultrasonics 4 (1966) 178–185.
[29] A.T. Male, Friction measurement using the ring compression test, Proceedings of the Seventh ICTP Conference, 2002, pp. 321–326.
[30] J. Hung, Y. Tsai, C. Hung, Frictional effect of ultrasonic-vibration on upsetting, Ultrasonics 46 (2007) 277–284.
[31] H. Huang, A. Pequegnat, B.H. Chang, M. Mayer, D. Du, Y. Zhou, Influence of superimposed ultrasound on deformability of Cu, J. Appl. Phys. 106 (2009) 113514.
[32] S. Bagherzadeh, K. Abrinia, Y. Liu, Q. Han, The effect of combining high-intensity ultrasonic vibration with ECAE process on the process parameters and mechanical properties and microstructure of aluminum 1050, Int. J. Adv. Manuf. Tech. 88 (2017) 229–240.
[33] B. Schinke, T. Malmberg, Dynamic tensile tests with superimposed ultrasonic oscillations for stainless steel type 321 at room temperature, Nucl. Eng. Des. 100 (1987) 281–296.
[34] X. Zhuang, J. Wang, H. Zheng, Z. Zhen, Forming mechanism of ultrasonic vibration assisted compression, T. Nonferr. Metal. Soc. 25 (7) (2015) 2352–2360.
[35] C. Yang, X. Shan, T. Xie, Titanium wire drawing with longitudinal-torsional composite ultrasonic vibration, Int. J. Adv. Manuf. Tech. 83 (2016) 645–655.
[36] T. Wen, L. Wei, X. Chen, C. Pei, Effects of ultrasonic vibration on plastic deformation of AZ31 during the tensile process, Int. J. Min. Met. Mater. 18 (2011) 70–76.
[37] D. Nouailhas, G. Cailletaud, H. Policella, D. Marquis, J. Dufailly, H. Lieurade, A. Ribes, E. Bollinger, On the description of cyclic hardening and initial cold working, Eng. Fract. Mech. 21 (1985) 887–895.
[38] Z. Xie, Y. Guan, L. Zhu, J. Zhai, J. Lin, Investigations on the surface effect of ultrasonic vibration-assisted 6063 aluminum alloy ring upsetting, Int. J. Adv. Manuf. Tech. 96 (2018) 4407–4421.